Int. J. Electrochem. Sci., 11 **(2016)** 10863 – 10873, doi: 10.20964/2016.12.91

International Journal of
ELECTROCHEMICAL
SCIENCE
www.electrochemsci.org

I Doping 1D $Li_4Ti_5O_{12}$ Nanofibers as Anode Materials for Lithium-Ion Battery

Kai Yang[1], *Zhanyu Li*[2], *Yuguang Zhao*[2], *Yudong Wang*[2], *Fei Gao*[1], *Jianling Li*[2,*]

[1] China electric power research institute, Beijing 100085, China.
[2] School of Metallurgical and Ecological Engineering, University of Science and Technology Beijing, No. 30 College Road, Beijing 100083, China.
[*]E-mail: lijianling@ustb.edu.cn

Received: 30 September 2016 / *Accepted:* 29 October 2016 / *Published:* 10 November 2016

One-dimensional (1D) nanostructures provide shortened Li^+ diffusion pathways, structural stability and large interfacial area between the active material and electrolyte, which enhances the reversibility and cycling performance of spinel $Li_4Ti_5O_{12}$ (LTO). Herein, we have successfully synthesized iodine (I) doping 1D LTO nanofibers by an electrospinning technique and studied the I doping effect on the lattice parameter, morphology and electrochemical properties of 1D LTO nanofibers. The 1D $Li_4Ti_5O_{12-x}I_x$ (x=0.3) nanofibers have excellent rate capability, specific capacity and cycling stability because of the shortened diffusion length for Li^+ transport, which are mainly due to cubic lattice parameter of LTO increase with I doping. Also, Cyclic voltammetry (CV) and Electrochemical impedance spectroscopy (EIS) results confirmed that I doping can reduce the electrochemical polarization of LTO and increase the lithium ion diffusion coefficient, which can improve the electrochemical performance of LTO.

Keywords: $Li_4Ti_5O_{12}$, Anode material, I-doping, Electrospinning, Lithium-ion battery

1. INTRODUCTION

Rechargeable Lithium ion batteries (LIB) have attracted much attention as the most promising energy storage devices, owing to their great advantages, such as high energy density, easy handling, high cell voltage, absence of a memory effect, long cycling life, and even benign towards the environment in comparison to other rechargeable batteries [1-3]. In particular, spinel $Li_4Ti_5O_{12}$ (LTO) have already been used in portable electronics, such as laptops and cameras, as well as electric vehicles (EVs) and plug-in hybrid electric vehicles (PHEVs) [4-5]. It is well known that this is mainly due to its two key advantages: (1) excellent reversibility and structure stability arising from its zero-strain

structure during lithium-ion intercalation and deintercalation [6]; (2) a higher equilibrium potential plateau (1.55 V *vs*. Li/Li^+), which can avoid the formation of SEI layers and prohibits lithium dendrite deposition on the surface of the electrode [7]. However, $Li_4Ti_5O_{12}$ has a low electrical conductivity (ca.10^{-13} S cm^{-1}) and lithium diffusion coefficient (ca.10^{-9} to 10^{-16} cm^2 s^{-1}), which results in poor rate capability and limits its use [8-9].

At present, a variety of methods have been employed to enhance the rate capability of $Li_4Ti_5O_{12}$ anodes, such as size control and surface modification [10-12]. In our previous work, we had synthesized TiN coated $Li_4Ti_5O_{12}$ submicrospheres by solvothermal method and subsequent nitridation process in the presence of ammonia [13]. The uniformly coated conducting TiN layer on the surface of LTO submicrospheres enhances the reversibility and cycling performance of LTO. In addition, ion doping is an effective approach to improve its rate capability. There are some of metallic elements such as Na, Mg, Ce, Ru, Dy, and Sm, etc. doping on the Li or Ti sites have been investigated constantly [12,14-18]. However, to the best of our knowledge, very few studies have focused on doping non-metal anions into O sites (such as I) to enhance electrochemical performance of LTO in addition to F [19], Cl [20] and Br [21].

As previously reported in the literature, one-dimensional (1D) nanostructures have remarkable electrical, thermal, and mechanical properties as promising anode structures in lithium rechargeable batteries [22]. The main reason is that 1D nanostructures provide shortened Li^+ diffusion pathways and large interfacial area between the electrolyte and the active material, and hence, improve electrochemical properties such as reversible capacity and rate capability [23]. Therefore, we hope to improve the electrochemical performance of LTO by the combination of 1D nanostructures and doping technology.

In this study, we have successfully synthesized 1D $Li_4Ti_5O_{12-x}I_x$ (x=0, 0.1, 0.3, 0.5) nanofibers by an electrospinning technique, which can readily fabricate 1D nanofibers with various diameters, compositions, and morphologies [24]. The effect of I doping on the electrochemical properties are investigated. Also, we successfully demonstrated that the 1D $Li_4Ti_5O_{12-x}I_x$ (x=0.3) nanofibers have excellent rate capability and cycling stability because of the shortened diffusion length for Li^+ transport and the fast electron transport.

2. EXPERIMENT

2.1. Sample preparation

1D $Li_4Ti_5O_{12-x}I_x$ (x=0, 0.1, 0.3, 0.5) nanofibers were synthesized by an electrospinning technique. In a typical synthesis, (0.05 mol) titanium (IV) isopropoxide, (0.039 mol) lithium acetate and (0.003 mol) lithium iodide were blended with a solution containing (18 mL) ethanol and (20 mL) acetic acid in a Li: Ti molar ratio of 0.84:1 for the 1D $Li_4Ti_5O_{12-x}I_x$ (x=0.3) nanofiber. LiI was used as iodine source and lithium source at the same time. Excess Li was provided to compensate for Li evaporation at high temperature during synthesis. After that, (1.8 g) polyvinylpyrrolidone (PVP, Mw=1,300,000,) was added in the above solution and magnetically stirred 12 h. The obtained solution was loaded into a plastic syringe equipped with a metallic needle with a diameter of 1.0 mm which was

connected to a high-voltage power supply. A piece of alumina foil was employed to collect the gel fibers. The distance between collector and the tip of the needle was 13 cm, the applied voltage between them was 20 kV and the feeding rate for the precursor was set to 2.5 $ml \cdot h^{-1}$. The electrospinning process was carried out at room temperature in air. The electrospun nanofibers were annealed at 800 °C in air for 10 h at a heating rate of 2°C/min in order to obtain 1D I-doped LTO nanofibers. For comparison, the undoped 1D LTO nanofibers were prepared by the same approach without LiI.

2.2. Material characterization

The crystal lattice parameters and phase composition of the synthesized powders were characterized by powder X-ray diffraction (XRD, Rigaku RINT2400 with Cu Kα radiation, λ=0.154056 nm, Japan) in 2θ degree range from 10° to 90° at a scanning rate of 10°/min. The morphology and microstructure of the as-synthesized 1D LTO and I-doped LTO nanofibers were observed using field-emission scanning electron microscopy (FESEM, Zeiss SuprATM 55, Germany) equipped with energy dispersive X-ray spectroscopy (EDS).

2.3. Electrode preparation

1D pure and I-doped LTO powders were thoroughly mixed with 10% polyvinylidene fluoride (PVDF) and 10% conductive carbon black in N-methyl-2-pyrrolidine (NMP) solution with a carnelian mortar, and then pasted on Cu foil using the doctor blade technique before the electrode was dried in a vacuum oven at 100 °C for 12 h. After that, the electrode with an active material loading of 1-2 $mg \cdot cm^{-2}$ was cut into circular pieces with a diameter of 10 mm as a working electrode. Pure lithium foil was used as the counter electrode, and Celgard 2400 as the separator. 1.0 $mol \cdot L^{-1}$ $LiPF_6$ in a volume ratio of 1:1 mixture of ethylene carbonate (EC) and dimethyl carbonate (DMC) was used as the electrolyte. Every coin cell was assembled in a glove box ($[O_2]$ <1 ppm, $[H_2O]$ <1 ppm) filled with high purity argon gas.

2.4 Electrochemical characterization

In order to study 1D pure and I-doped LTO nanofibers electrochemical properties, the galvanostatic charge-discharge tests were carried out using a Land battery test system (CT2001A Wuhan, China) over a voltage of 1.0-2.5 V at room temperature. The rate capability of the 1D LTO and I-doped LTO samples was performed at different rates of 0.2C (35 $mA \cdot g^{-1}$), 1C (175$mA \cdot g^{-1}$), 5 C (875$mA \cdot g^{-1}$), 10 C (1750 $mA \cdot g^{-1}$) and 20 C (3500 $mA \cdot g^{-1}$). The cycling tests were conducted at 5C. The cyclic voltammetry (CV) was carried out on a VMP2 electrochemical workstation at a scan rate of 0.5 mV·s-1 in the potential range of 1.0-2.5 V (*vs.* Li/Li^+). The electrochemical impedance spectroscopy (EIS) measurements were performed using a VMP2 electrochemical system. The spectra were potentiostatically measured by applying an ac voltage of 10 mV over the frequency range of 100 kHz to 10 mHz.

3. RESULTS AND DISCUSSION

X-ray diffraction (XRD) results of the pure 1D LTO nanofibers and the I-doped LTO nanofibers are shown in Fig.1. Among the four samples, the major diffraction peaks are in accordance with the standard diffraction pattern of LTO (JCPDS No. 49-0207). The XRD result reveals that pure phase of 1D LTO material nanofibers was successfully synthesized via an electrospinning technique. Also, no impurity peak in the XRD pattern was found for the 1D I-doped LTO nanofibers, which indicates that the dopant I has entered the lattice structure of 1D LTO nanofibers without causing any changes in its structural characteristics. However, the diffraction peaks of the 1D I-doped LTO nanofibers exhibit numerous slight shifts toward lower 2θ. In order to clear observation, the peak positions of (111) planes of the 1D I-doped LTO nanofibers are magnified and shown in Fig. 1b. The lattice parameters were calculated from the XRD fitting results, and the obtained data are listed in Table 1. It can be seen from the Table 1 that the cubic lattice parameter increases with increasing I doping, as x increases from 0 to 0.5. The increase of the lattice constant can be attributed to the following two reasons. On one hand, I ion (2.2 Å) with a lager ionic radius substitution for O ion (1.4 Å) in the 32e sites; on the other hand, the lager Ti^{3+} (0.67 Å) distributed at octahedral 16d sites could randomly occupy the 8b, 48f or 16c sites to provide the charge compensation due to I modifying [19, 25].

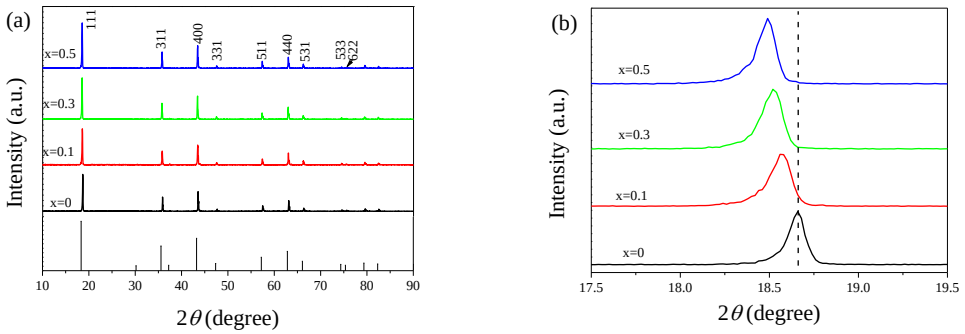

Figure 1. a) XRD patterns of the 1D LTO and I-doped LTO nanofibers, and enlarged views of the b) LTO (111) peaks.

Table 1. Variation in crystal lattice parameter for the 1D LTO and I-doped LTO nanofibers

Sample	Lattice parameter (Å)
x=0	8.348
x=0.1	8.359
x=0.3	8.364
x=0.5	8.368

The morphologies of the 1D $Li_4Ti_5O_{12-x}I_x$ (x=0, 0.1, 0.3, 0.5) nanofibers were characterized by Scanning electron microscopy (SEM) as shown in Fig.2. The SEM images reveal that both nanofibers have identical 1D nanofibers morphology. The nanofibers have an average diameter of ~200 nm and

continuous 1D geometry. Therefore, we can get from the Fig.2 that I-doping did not obviously change the morphologies of the 1D LTO nanofibers. The distribution and content of 1D $Li_4Ti_5O_{12-x}I_x$ (x=0.3) nanofibers was investigated by energy dispersive spectroscopy (EDX) and the results are shown in Fig. 3. The EDS mapping results show that the O, Ti and I are uniformly distributed in the 1D $Li_4Ti_5O_{12-x}I_x$ (x=0.3) nanofibers. The above results confirm that the O site at the 32e sites might be successfully occupied by the I by an electrospinning technique.

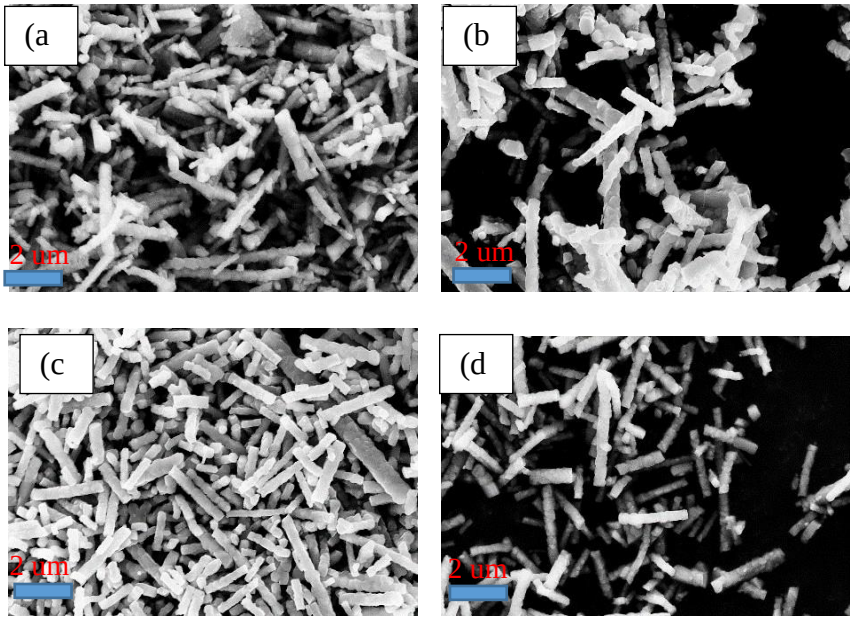

Figure 2. SEM images of the 1D $Li_4Ti_5O_{12-x}I_x$ (x = 0, 0.1, 0.3, 0.5) nanofibers: (a) x = 0, (b) x = 0.1, (c) x = 0.3, and (d) x = 0.5.

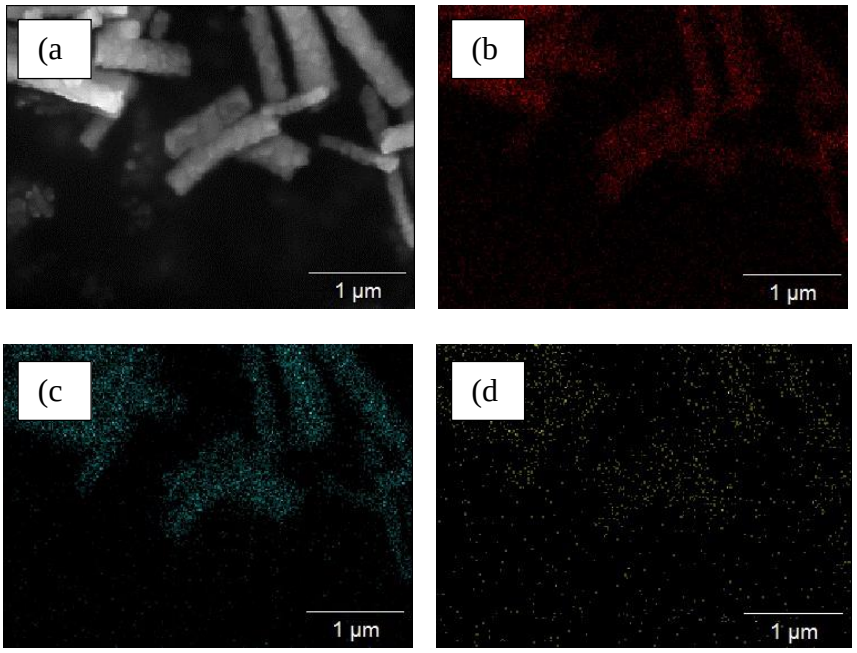

Figure 3. Energy dispersive analysis and element mapping of O (b), Ti (c) and I (d) on the 1D $Li_4Ti_5O_{12-x}I_x$ (x=0.3) nanofibers.

Electrochemical performances of the 1D pure LTO and the I-doped LTO nanofibers electrodes were tested using 2025 half-coin cells at the potential window of 1.0-2.5 V *vs*. Li/Li^+. Fig. 4a shows the rate capability of the 1D $Li_4Ti_5O_{12-x}I_x$ (x=0, 0.1, 0.3 and 0.5) samples at different rates of 0.2 C (35 $mA\cdot g^{-1}$), 1 C (175 $mA\cdot g^{-1}$), 5 C (875 $mA\cdot g^{-1}$), 10 C (1750 $mA\cdot g^{-1}$) and 20 C (3500 $mA\cdot g^{-1}$). The charge–discharge processes for each stage are taken for 3 cycles. It can be obviously seen from the Fig.4a that the discharge capacity decreases significantly as the discharge current rate increases from 0.2 C to 20 C. However, the 1D $Li_4Ti_5O_{12-x}I_x$ (x=0.3) nanofiber samples obtained by an electrospinning technique shows the best high-rate capability in the all samples. The discharge capacities of the1D pure LTO sample at 0.2 C, 1 C, 5 C, 10 C, and 20 C charge-discharge rate are 170.1 $mAh\cdot g^{-1}$, 130.5 $mAh\cdot g^{-1}$, 78 $mAh\cdot g^{-1}$, 59.9 $mAh\cdot g^{-1}$ and 47.3 $mAh\cdot g^{-1}$, respectively. While in case of the 1D $Li_4Ti_5O_{12-x}I_x$ (x=0.3) nanofiber sample, its rate performance is better than that of the pure LTO, the discharge capacities are 173.3 $mAh\cdot g^{-1}$, 143.1 $mAh\cdot g^{-1}$, 81.5 $mAh\cdot g^{-1}$, 62.9 $mAh\cdot g^{-1}$, and 55 $mAh\cdot g^{-1}$ at 0.2 C, 1 C, 5 C, 10 C, and 20 C charge-discharge rate, respectively. It may be attributed to that lattice parameter increases because of I ions doping as the above XRD confirmed will improve Li^+ intercalation and de-intercalation rate between the electrode and the electrolyte. Therefore, we can get that the doping of I ions improves the rate performance of 1D LTO nanofibers. Also, for the 1D $Li_4Ti_5O_{12-x}I_x$ (x=0.3) nanofiber sample, a stable capacity of 173 $mAh\cdot g^{-1}$ can be obtained without any decay as the current rate returned to 0.2 C from 20 C after 15 cycles, demonstrating that The reversibility and stability of LTO are not affected by I doping.

Fig. 4b and 4c compare charge/discharge voltage profiles of the 1D pure LTO and $Li_4Ti_5O_{12-x}I_x$ (x=0.3) samples at various current rates from 0.2 C to 20 C in the voltage range of 1.0-2.5 V *vs*. Li/Li^+. Both electrodes display distinct potential plateaus around 1.55 V (*vs*. Li/Li^+) at different rates from 0.5 C to 20 C, corresponding to the two-phase intercalation and de-intercalation reaction between $Li_4Ti_5O_{12}$ and $Li_7Ti_5O_{12}$ [26]. In the $Li_4Ti_5O_{12}$ structure, the tetrahedral 8a sites are occupied by three fourths of Li^+ ions, the rest of Li^+ ions and Ti^{4+} are distributed at octahedral 16d sites, while O^{2-} occupy the 32 e sites, and the 8 b, 48 f, and 16 c sites are empty [20]. During the intercalation process, three external Li^+ ions are embedded into the vacant 16c sites, which will make spinel $Li_4Ti_5O_{12}$ transform to rock-salt $Li_7Ti_5O_{12}$. It is clearly observed from the Fig.4b and 4c that the discharge plateau decreases with increasing the charge-discharge current density and the charge platform increases at the same rate, indicating that the polarization between the electrode and the electrolyte is increasing as the rate increasing. In the case of 1D $Li_4Ti_5O_{12-x}I_x$ (x=0.3) nanofiber, its voltage difference between the charge and discharge platform increases faster than that of 1D pure LTO with increasing the charge-discharge rate. In order to clearly observe the polarization between the electrode and the electrolyte, the polarization of ΔE versus discharge rate of the 1D pure LTO and $Li_4Ti_5O_{12-x}I_x$ (x=0.3) nanofibers electrodes are shown in Fig.4d. It is noticed from the Fig. 4d that the 1D $Li_4Ti_5O_{12-x}I_x$ (x=0.3) nanofiber shows lower ΔE value than that of pure LTO at the same charge-discharge current density, suggesting that I doped LTO makes the polarization resistance significantly decrease and favors the improvement of the rate capabilities.

The cycling performances and coulombic efficiency of the 1D pure LTO and $Li_4Ti_5O_{12-x}I_x$ (x=0.3) nanofibers at the current density of 875 $mAh\cdot g^{-1}$ over 100 cycles are shown in Fig. 4e. We can find from the image that the coulombic efficiency of the both samples in this 100 charge-discharge

cycles remains almost constant at about 100%. It can be also seen that the discharge capacity of the both samples can be obtained without any decay after 100 cycles, which can be attributed to the zero strain characteristics of LTO during lithium-ion insertion and extraction.

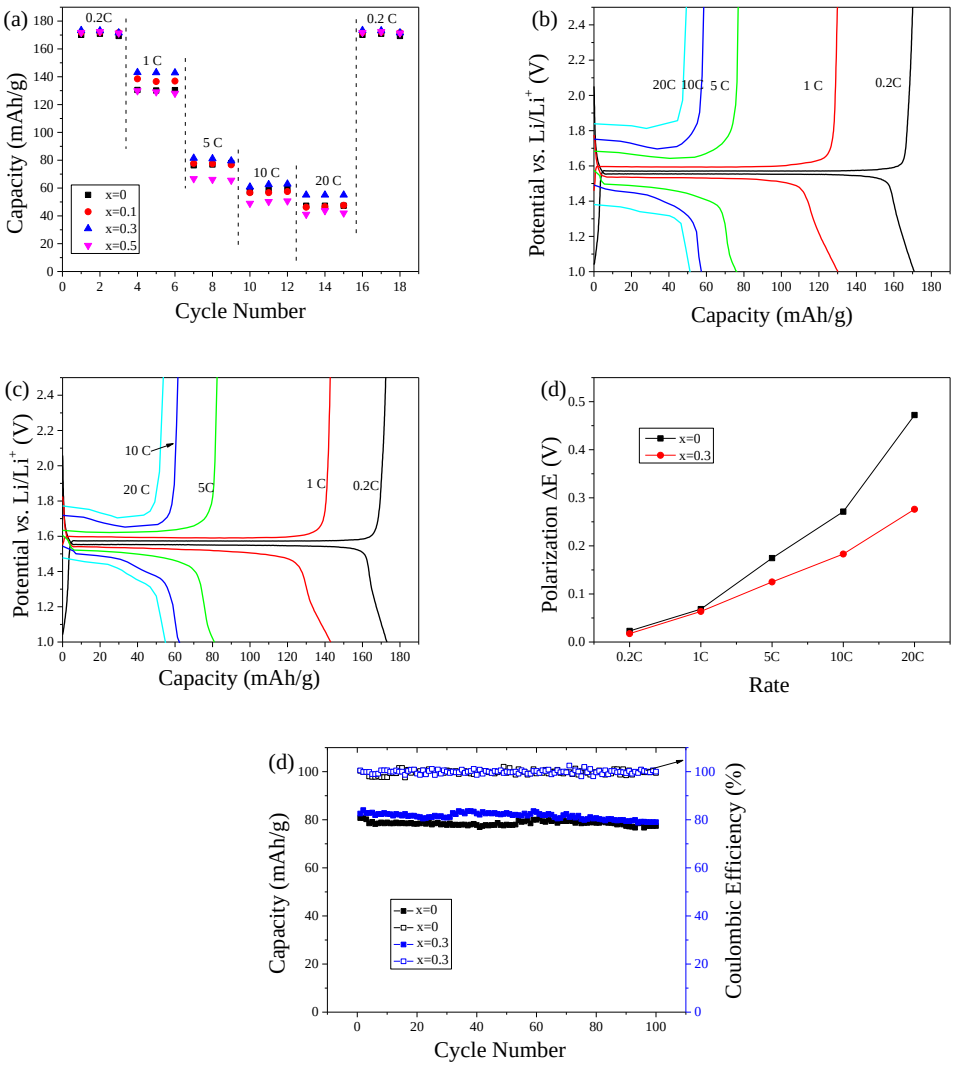

Figure 4. (a) The rate performance of the 1D pure LTO and the I-doped LTO nanofibers at the different charge-discharge rate; The initial charge-discharge curves of (b) 1D pure LTO and (c) I-doped LTO nanofibers; (d) The plots of *ΔE* of the samples versus C rates; (e) The cycling performances of 1D pure LTO and $Li_4Ti_5O_{12-x}I_x$ (x=0.3) nanofibers at a rate of 5C.

In order to confirm the effect of I doping on the redox reaction of LTO, the cyclic voltammograms (CVs) of the 1D pure LTO and $Li_4Ti_5O_{12-x}I_x$ (x=0.3) nanofibers as active materials at the scanning rate of 0.5 $mV \cdot s^{-1}$ between 1.0 and 2.5 V are shown in Fig. 5. It can be seen from Fig. 5 that the CVs of both investigated electrodes are almost the same, and they show one cathodic peak located at 1.47 V (*vs.* Li/Li^+), corresponding to Li^+ insertion into spinel $Li_4Ti_5O_{12}$ anode [27]. They also show an anodic peak at 1.69 V (*vs.* Li/Li^+), representing the Li^+ extraction from rock-salt $Li_7Ti_5O_{12}$. As we know, the potential differences between anodic and cathodic peaks reflect the degree

of polarization of the electrodes [28]. The potential differences of both samples are given in Table 2. It can be seen that the potential differences between the anodic and cathodic peaks for the 1D $Li_4Ti_5O_{12-x}I_x$ (x=0.3) nanofiber electrode is lower than that of 1D pure LTO. This reveals that I doping is beneficial for the reversible insertion and extraction of Li^+ and reduces the electrode polarization between the electrode and the electrolyte, which is consistent with the results obtained in Fig. 4d. It is well-known that the ratio of anodic peak current to cathodic peak current (I_{pa}/I_{pc}) is an important parameter to embody the reversibility of the Li^+ insertion-extraction process [29-30]. The I_{pa}/I_{pc} values of the 1D pure LTO and $Li_4Ti_5O_{12-x}I_x$ (x=0.3) nanofibers between 1.0 and 2.5 V (*vs*. Li/Li^+) at scan rates of 0.5 $mV \cdot s^{-1}$ are also listed in Table 2. It is clearly observed that the I_{pa}/I_{pc} value of the 1D $Li_4Ti_5O_{12-x}I_x$ (x=0.3) nanofiber electrode is smaller than that of 1D pure LTO, suggesting that I doping enhances the reversibility and cycling performance of LTO. As a result, it can be estimated that the 1D $Li_4Ti_5O_{12-x}I_x$ (x=0.3) nanofiber electrode possess more excellent kinetics and faster Li^+ diffusion path than that of pure LTO.

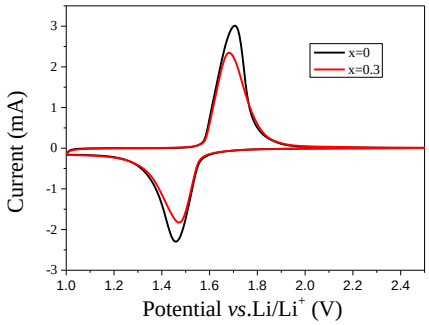

Figure 5. CV curves of the 1D pure LTO and $Li_4Ti_5O_{12-x}I_x$ (x=0.3) nanofibers at the scanning rate of 0.5 $mV \cdot s^{-1}$.

Table 2. Potential difference between anodic and cathodic peaks and the I_{pa}/I_{pc} values of the 1D pure LTO and $Li_4Ti_5O_{12-x}I_x$ (x=0.3) nanofibers.

Sample	φ_a /V	φ_c /V	$(\varphi_a - \varphi_c)mV$	I_{pa}/mA	I_{pc}/mA	I_{pa}/I_{pc}
X=0	1.707	1.466	241	3.013	2.281	1.32
X=0.03	1.679	1.472	207	2.346	1.831	1.28

In order to confirm the effect of I doping on the transport kinetics of lithium ions, the electrochemical impedance spectra (EIS) for the 1D pure LTO and $Li_4Ti_5O_{12-x}I_x$ (x=0.3) nanofibers are conducted on the coin batteries with a frequency range from 1×10^5 to 0.01 Hz, and the corresponding Nyquist plots are shown in Fig. 6. It can be seen from the figure that the plots are similar in shape, with a semicircle at the high frequency region and a straight line with a slope close to 45° at the low frequency domain [31]. The semicircle in the high frequency region is mainly related to the charge transfer resistance (R_{ct}), and the inclined straight line in the low frequency domain is ascribed to the Warburg impedance caused by a semi-infinite diffusion of Li^+ ion in the electrode [32]. The

corresponding equivalent circuit is given in the inset of Fig. 6, in which W is the Warburg impedance, CPE is the constant phase element related to the interfacial capacitance, R_{ct} is the charge transfer resistance, and R_s is the ohmic resistance from electrolyte [33].

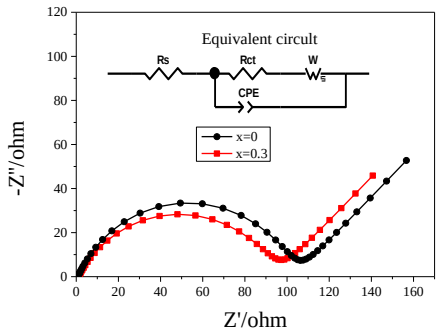

Figure 6. Nyquist plots of the 1D pure LTO and $Li_4Ti_5O_{12-x}I_x$ (x=0.3) electrodes at an anodic potential of 1.55V (*vs* Li/Li^+) from 100kHz to 10mHz.

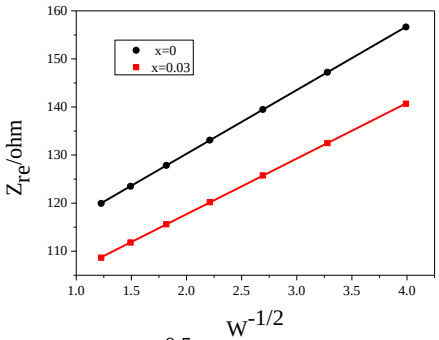

Figure 7. Graph of Z_{re} plotted against $w^{-0.5}$ at the frequency region for the 1D pure LTO and $Li_4Ti_5O_{12-x}I_x$ (x=0.3) electrodes.

The information acquired from the fitted EIS using the equivalent circuit is listed in Table 3. It can be found from the Table 3 that the charge transfer resistance of the 1D $Li_4Ti_5O_{12-x}I_x$ (x=0.3) nanofiber electrode is 94.22 Ω, while that of the 1D pure LTO electrode is 103.40 Ω. This indicates that an appropriate amount of I dopant is favorable to reduce the charge transfer resistance of LTO. The main reason can be attributed to I^- substitution for O^{2-} in LTO, which will cause the generation of mixing valence of Ti^{3+}/Ti^{4+} as charge compensation [34].

The lithium ion diffusion coefficient (D_{Li}) can be calculated from the plots according to the following equations: [32, 35]

$$Z_{re} = R_{ct} + R_s + \sigma\omega^{-\frac{1}{2}} \qquad (1)$$

$$D_{Li} = \frac{(RT)^2}{2A^2n^4F^4C_{Li}^2\sigma^2} \qquad (2)$$

where R is the gas constant, T is the absolute temperature, A is the surface area of electrode, n is the number of electrons transferred in the half-reaction for the redox couple, F is the Faraday constant, C_{Li} is the concentration of lithium ions, and σ is the Warburg factor, which is related to Z_{re}

according to equation (2), and can be obtained from the slope of $Z_{re} \sim \omega^{-1/2}$ plot as shown in the inset of Fig. 7 [36].

Table 3. Parameters of the EIS for the 1D pure LTO and $Li_4Ti_5O_{12-x}I_x$ (x=0.3) electrodes.

Sample	R_s/Ω	R_{ct}/Ω	$D_{Li}/cm^2 s^{-1}$
X=0	0.91	103.40	1.71×10^{-11}
X=0.3	1.08	94.22	2.24×10^{-11}

The calculated results of both samples are also listed in Table 3. It can be seen that the 1D $Li_4Ti_5O_{12-x}I_x$ (x=0.3) nanofiber electrode have better diffusion coefficient than that of the 1D pure LTO electrode. This result clearly indicates that I doping could enhance the Lithium-ion diffusion and decrease the charge transfer resistance, which is beneficial for improve the electrochemical performance of LTO in terms of charge-discharge capacity and rate capability.

4. CONCLUSIONS

In this paper, we have successfully prepared 1D $Li_4Ti_5O_{12-x}I_x$ (x=0, 0.1, 0.3 and 0.5) nanofibers by an electrospinning technique, which is an effective way to improve the kinetics of 1D LTO toward fast Li^+ intercalation/de-intercalation. The structural structure, morphology and electrochemical performance of $Li_4Ti_5O_{12-x}I_x$ (x=0, 0.1, 0.3 and 0.5) were investigated. I doping in the LTO lattice barely changed the fiber dimensions, but it increased the lattice constant, reversibility and Li^+ diffusion coefficient as proved by FESEM, XRD, CV and EIS. Among the I-doped samples, the 1D $Li_4Ti_5O_{12-x}I_x$ (x=0.3) exhibits superior rate capability, specific capacity and cycling stability due to higher conductivity and faster Li^+ diffusion compared with the 1D pure LTO. Therefore, the excellent electrochemical properties of LTO can be obtained by the combination of 1D LTO nanofibers and I doping technology.

ACKNOWLEDGEMENTS
The work was financially by the science and technology project of State Grid Corporation of china (DG71-15-042).

References

1. G. Jeong, Y.U. Kim, H. Kim, Y.J. Kim, H.J. Sohn, *Energy Environ. Sci.*, 4 (2011) 1986-2002.
2. M. Armand, J.M. Tarascon, *Nature*, 451 (2008) 652–657.
3. L.W. Ji, Z. Lin, M. Alcoutlabi, X.W. Zhang, *Energy Environ. Sci.*, 4 (2011) 2682-2699.
4. B. Dunn, H. Kamath, J.M. Tarascon, *Science*, 334 (2011) 928-935.
5. L. Kavan, M. Gratzel, *Solid-State Lett.*, 5 (2002) A39–A42.
6. X. Lu, L. Zhao, X. He, R. Xiao, L. Gu, Y.S. Hu, H. Li, Z. Wang, X. Duan, L. Chen, *Adv. Mater.*, 24 (2012) 3233–3268.
7. Z.Y. Jia, Q. Zhou, X.W. Li, Y. Fu, H. Ming, J.W. Zheng, *Electrochim. Acta*, 156 (2015) 216-222.

8. C.Y. Ouyang, Z.Y. Zhong, M.S. Lei, *Electrochem. Commun.*, 9 (2007) 1107-1112.
9. P.C. Tsai, W.D. Hsu, S.K. Lin, *J. Electrochem. Soc.*, 161 (2014) A439-A444.
10. W. Liu, Q. Wang, J. Zhang, X.H. Xie, H.H. Liu, G.Q. Min, G.Q. Xia, *Volume*, 287 (2016) 373-379.
11. Z.K. Fang, Y.R. Zhu, T.F. Yi, Y. Xie, *ACS Sustainable Chem. Eng.*, 4 (2016) 1994−2003.
12. Q.Y. Zhang, Y. Liu, H.S. Lu, D.P. Tang, C.Y. Ouyang, L.Z. Zhang, *Electrochimi. Acta*, 189 (2016) 147–157.
13. Z.Y. Li, F.X. Ding, Y.G. Zhao, Y.D. Wang, J.L. Li, K. Yang, F. Gao, *Ceram. Int.*, 42 (2016) 15464-15470.
14. F. Zhao, P. Xue, H.H. Ge, L. Li, B.F. Wang, *J. Electrochem Soc.*, 5 (2016) A690-A695.
15. W. Wang, H.L. Wang, S.B. Wang, Y.J. Hu, Q.X. Tian, S.Q. Jiao, *J. Power Sources*, 228 (2013) 244–249.
16. F.Y. Li, M. Zeng, J. Li, H. Xu, *Int. J. Electrochem. Sci.*, 12 (2015) 10445–10453.
17. K.Q. Ding, J. Zhao, J.M. Zhou, Y.B. Zhao, Y.Y. Chen, Y. Zhang, B.J. Wei, L. Wang, X.M. He, *Int. J. Electrochem. Sci.*, 1 (2016) 446-458.
18. Z.Y. Li, J.L. Li, Y.G. Zhao, K. Yang, F. Gao, X. Li, *RSC Adv.*, 6 (2016) 15492–15500.
19. Z. Zhao, Y.L. Xu, M.D. Ji, H. Zhang, *Electrochim. Acta*, 109 (2013) 645-650.
20. Y.D. Huang, Y.L. Qi, D.Z. Jia, X.C. Wang, Z.P. Guo, W. Cho, *J. Solid State Electrochem.*, 16 (2012) 2011–2016.
21. Q.Y. Zhang, H.S. Lu, H.X. Zhong, X.D. Yan, C.Y. Ouyang, L.Z. Zhang, *J. Mater. Chem. A*, 3 (2015) 13706-13716.
22. J.G. Kim, D. Shi, K.J. Kong, Y.U. Heo, J.H. Kim, M.R. Jo, Y.C. Lee, Y.M. Kang, S.X. Dou, *ACS Appl. Mater. Inter.*, 5 (2013) 691–696.
23. X. Lu, C. Wang, Y. Wei, *Small*, 5 (2009) 2349-2370.
24. S. Cavaliere, S. Subianto, I. Savych, D.J. Jones, J. Roziere, *Energy Environ. Sci.*, 4 (2011) 4761–4785.
25. S. Scharner, W. Weppner, P. Schmid-Beurmann, *J. Electrochem. Soc.*, 146 (1999) 857–861.
26. D. Pal, J.L. Pandey, *Bull. Mater. Sci.*, 33 (2010) 691-696.
27. Y.Y. Zhang, C.M. Zhang, Y. Lin, D.B. Xiong, D. Wang, X.Y. Wu, D.N. He, *J. Power Sources*, 250 (2014) 50-57.
28. L.P. Fan, X. Tan, T. Yu, Z.Q. Shi, *RSC Adv.*, 6 (2016) 26406-26411.
29. Z.N. Wan, R. Cai, S.M. Jiang, Z.P. Shao, *J. Mater. Chem.*, 22 (2012) 17773-17781.
30. Z.Y. Li, J.L. Li, Y.G. Zhao, K. Yang, F. Gao, X. Li, *Ionics*, 22 (2016) 789–795.
31. L. Yang, L. Gao, *J. Alloys Compd.*, 485 (2009) 93-97.
32. W.J. Zhu, H. Yang, W.K. Zhang, H. Huang, X.Y. Tao, Y. Xia, Y.P. Gan, X.Z. Guo, *RSC Adv.*, 5 (2015) 74774-74782.
33. A.Y. Shenouda, K.R. Murali, *J. Power Sources*, 214 (2012) 220-226.
34. H. Zhao, Y. Li, Z. Zhu, J. Lin, Z. Tian, R. Wang, *Electrochim. Acta*, 53 (2008) 7079–7083.
35. J. Chen, L. Yang, S. Fang, S.i. Hirano, K. Tachibana, *J. Power Sources*, 200 (2012) 59-66.
36. C. Wang, S. Wang, L.K. Tang, Y.B. He, L. Gan, J. Li, H.D. Du, B.H. Li, Z.Q. Lin, F.Y. Kang, *Nano Energy*, 21 (2016) 133–144.